FLOW-INDUCED VIBRATION OF A SPHERE UP TO CRITICAL REYNOLDS NUMBER

Takashi Nishihara & Yuzuru Eguchi
Fluid Dynamics Sector, Civil Engineering Research Laboratory, Central Research Institute of Electric Power Industry, 1646 Abiko, Abiko-shi, Chiba 270-1194, Japan

ABSTRACT

This paper describes the dynamic behavior of a sphere tethered in a vertical water tunnel at critical and subcritcal Reynolds numbers. A 2 m×2 m square-section water tunnel and two sphere models of diameter 0.2 m and 0.4 m were used. The mass ratio was about 1.5 and the mass damping parameter was close to 0. Violent vibrations with large amplitudes in excess of 4.5 times the sphere diameter were observed at the critical Reynolds number. The behavior at subcritical Reynolds numbers was similar to that reported in several previous studies.

1. INTRODUCTION

When designing structures subject to flow, it is desirable to evaluate flow-induced vibrations (FIV) to confirm their long-term integrity. Many studies have been conducted on the FIV of cylindrical structures due to their practical importance, as comprehensively reviewed by King (1977), Sarpkaya(1979, 2004), Bearman (1984), Naudascher (1987), Matsumoto (1999), Williamson et al. (2004), etc. They are also summarized in the books of Chen (1987), Blevins (1990), Naudascher and Rockwell (1994), and others.

FIV of a sphere has also been studied by several researchers. Williamson et al. (1997) investigated the behavior of a tethered sphere in a horizontal water channel for the case of low structural damping and low mass ratio. They found that vortex-induced vibration (VIV) can be caused in the above system. Furthermore, the vibration amplitude depends mainly on the reduced velocity $U^* = U/(f_n d)$; where: U, f_n and d are the incidence flow velocity, the natural frequency in the fluid and the diameter of a sphere, respectively. They also showed that the Reynolds number and tether length have little effect on the response amplitude. Jauvtis et al. (2001) conducted similar experiments in a horizontal wind tunnel for high mass ratios. In addition to the known VIV mode observed in the range of $4 \leq U^* \leq 12$, they found two new vibration modes in the higher reduced velocity range. One is another periodic vibration appearing in the reduced velocity range of $20 \leq U^* \leq 40$. The other is intermittent bursts of large amplitude vibration for $U^* > 100$. Provansal et al. (2005) conducted experiments on a tethered sphere in a vertical water tunnel and observed VIV with circular or elliptical trajectories in the plane perpendicular to the flow. Govardhan et al. (2005) conducted free-vibration tests on both a tethered sphere and an elastically supported sphere in a flow, and deduced that there exists a critical mass ratio, below which large amplitude VIV continues to infinite U^*. These previous studies however were limited to subcritical Reynolds numbers. FIV of a sphere at high Reynolds number is not yet fully understood.

In this study, free-vibration tests on a sphere tethered in a vertical water tunnel were conducted up to critical Reynolds number.

2. EXPERIMENTAL SETUP

Figure 1 shows schematically the experimental arrangement employed herein.

A large-scale gravity-driven vertical water tunnel in CRIEPI (Nishihara et al., 1998) was used for the tests. The water tunnel system consists of a 1000 m^3 underground reservoir, an upper circular head tank of 3 m height and 12 m diameter, a vertical water tunnel section and four control valves for draining. The test section is 2 m×2 m square. In preparation for use of the tunnel, the valves are closed and water is pumped from the underground reservoir into the head tank. When the water level in the head tank reaches the prescribed level, the pump is stopped. When the valves are opened, gravity induces the water to flow down thorough the test-section and into the underground reservoir. The extent to which the valves are opened controls the flow rate. The descent rate of the water level in the

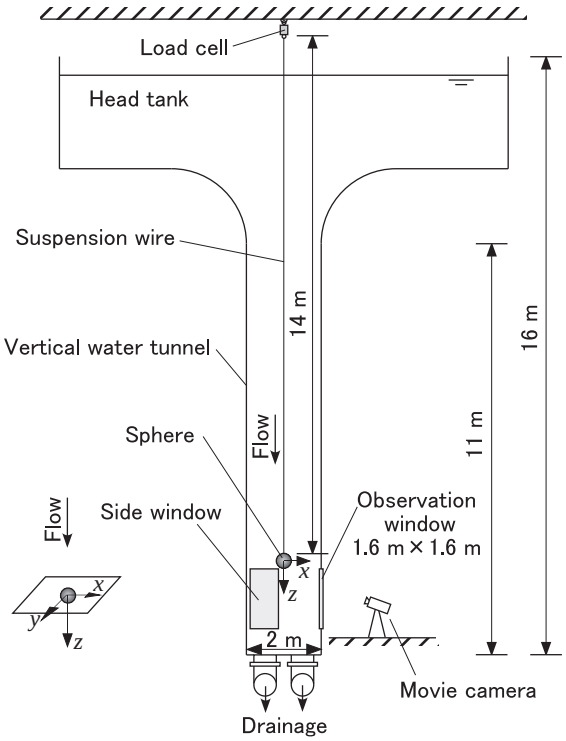

Figure 1: *Schematic arrangement of the experimental setup.*

head tank, as measured by a water level gauge (CHT4-300, KENEK), was correlated to the incident flow velocity using preliminary Pitot tube measurements. During the free-vibration tests, the flow velocity was obtained from the descent rate of the head tank water level.

In the tests, a sphere model was suspended from a load cell (LTZ-50KA or LTZ-200KA, KYOWA) fixed to one of the laboratory roof beams and located in the center of the water tunnel test section. Stainless steel wire of 14 m length and either 1.5 mm or 3 mm diameter was used to suspend the sphere. The sphere model represents a pendulum in both the x and y directions, as shown in Fig. 1. The motion of the sphere was recorded using a digital movie camera, and the vibration amplitude and frequency were obtained from these movies. It should be noted that the camera was set as shown in Fig.1. Consequently, only the y-direction vibration amplitude was estimated. During the tests, the drag force on the sphere was also measured using the load cell.

Two sphere models were used for the tests. Both spheres were smooth stainless steel shells filled with mortar and plastic resin. Table 1 shows the specifications of the models and the experimental conditions. Table 2 shows a comparison between the conditions for the experiments herein and those for previous studies by

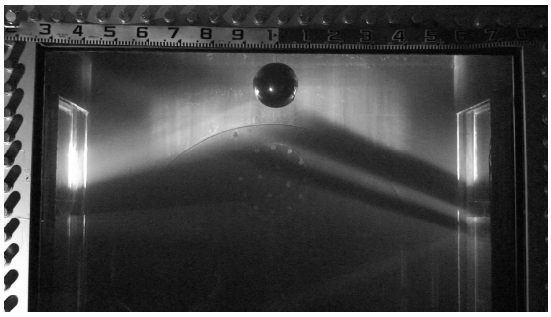

Figure 2: *Sphere model B in situ.*

Table 1: *Sphere model specifications and experimental conditions.*

	Model A	Model B
Diameter d [m]	0.4	0.2
Mass m_s [kg]	51	5.9
Mass ratio m^*	1.5	1.4
Wire length L [m]	14	14
Wire diameter [mm]	3	1.5
Natural period in the water T_{nw} [s]	14.9	16.3
Damping ratio ζ_{sw}	1.6×10^{-4}	8×10^{-4}
Flow velocity U[m/s]	0.05∼0.9	0.04∼2.0
Reduced velocity U^*	$1.9 \sim 35$	$3.4 \sim 160$
Reynolds number Re	$\sim 3 \times 10^5$	$\sim 4 \times 10^5$

other researchers. The mass ratio m^*, the relative tether length L^*, the reduced velocity U^*, and the Reynolds number Re in the tables are defined:

$$m^* = m_s/m_d, \quad m_d = \rho_w \pi d^3/6, \tag{1}$$

$$L^* = L'/d, \quad L' = L + d/2, \tag{2}$$

$$U^* = U/(f_{nw} d), \tag{3}$$

$$Re = Ud/\nu \tag{4}$$

where m_d is the displaced fluid mass, and ρ_w and ν are the density and kinematic viscosity of water, respectively.

Neglecting the added mass of air, the natural frequency f_{na} of the pendulum system in air can be expressed:

$$f_{na} = \frac{1}{2\pi}\sqrt{\frac{g}{L'}} \tag{5}$$

In preliminary tests, the free vibration frequency of a sphere in air agreed well with the above equation. Taking account of the buoyancy force and added mass, the natural frequency f_{nw} in water was estimated from:

$$f_{nw} = \frac{1}{2\pi}\sqrt{\frac{g}{L'}\frac{m^* - 1}{m^* + C_A}} \tag{6}$$

Table 2: *Comparison of experimental conditions for a tethered sphere.*

	Test section	m^*	L^*	Max. Re
Experiments herein	Vertical water tunnel	1.4, 1.5	35.5, 70.5	4×10^5
Williamson et al. (1997)	Horizontal water channel	0.082, 0.73	3.83 - 9.28	1.2×10^4
Jauvtis et al. (2001)	Horizontal wind tunnel	80, 940		10^5
Provansal et al. (2005)	Vertical water tunnel	2.43	9, 21	9×10^2
Provansal et al. (2005)	Horizontal wind tunnel	55.8, 61.7	2	6×10^2
Govardhan et al. (2005)	Horizontal water channel	0.45	5.9, 13.8	1.2×10^4

where C_A is the added mass coefficient and, for a sphere, is 0.5. The natural period in Table 1 is the reciprocal of the natural frequency.

The structural damping ratio ζ_{sa} was obtained from the pendulum motion decay rate in air and was about 2×10^{-4} and 1×10^{-3} for models A and B, respectively. Taking the added mass into account, the structural damping ratio ζ_{sw} in water was estimated to be 1.6×10^{-4} and 8×10^{-4} for models A and B, respectively. The mass damping parameters $m^*\zeta_{sw}$ were close to 0.

According to Achenbach (1972), the critical Reynolds number for a stationary sphere is 3.7×10^5. The maximum Reynolds number in the tests herein was 4×10^5, thus exceeding the critical Reynolds number.

Figure 2 shows an in situ photograph of the smaller sphere model B.

3. EXPERIMENTAL RESULTS

3.1. Results for the large sphere model A

Figure 3 shows the relative amplitude A_y^*; where: $A_y^* = A_y/2d$ and, in turn, A_y is the peak-to-peak amplitude of the sphere vibration obtained from the recorded movies over several cycles. The abscissas show both the reduced velocity U^* and the Reynolds number Re.

At $U^* = 1.9$, the sphere was almost at rest. For $U^* > 4$, the sphere started to vibrate and performed circular or elliptical trajectories in the x-y plane. This agrees with the results of previous studies and the observed behavior is probably VIV. Up to $U^* < 22$, similar vibrations were observed; the vibration amplitude gradually increasing with reduced velocity. The relative amplitude seems to saturate at about 1.5. However, further increase of the reduced velocity results in a sudden increase in vibration amplitude. Furthermore, in the cases of $Re > 2 \times 10^5$, the sphere contacts the side wall repeatedly. This suggests that the maximum vibration amplitude is well in excess of double the sphere diameter.

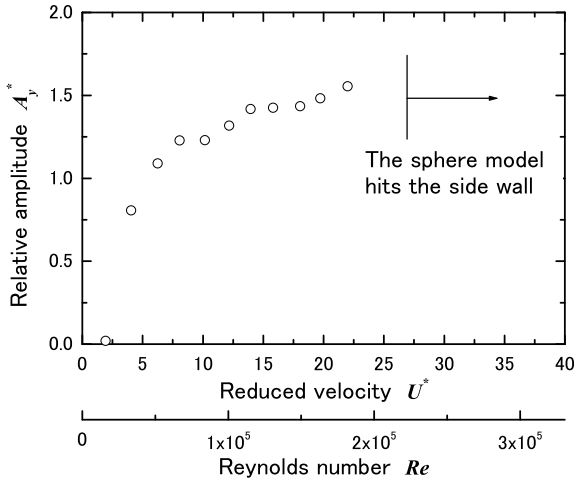

Figure 3: *Response amplitude of sphere model A.*

Figure 4 shows the mean drag coefficient $\bar{C}_D$ measured during the tests. $\bar{C}_D$ is defined:

$$\bar{C}_D = \bar{F}_D / \left(\tfrac{1}{2} \rho_w U^2 A_\perp \right), \quad A_\perp = \pi d^2/4 \qquad (7)$$

where $\bar{F}_D$ is the mean drag on a sphere. For $Re < 5 \times 10^4$, the drag force on the sphere is less than 1/2000 of the rated capacity of the load cell and reliable output could not be obtained. For $5 \times 10^4 < Re < 1.5 \times 10^5$, the mean drag coefficient was 0.7∼0.8, which is larger than that for a stationary sphere at subcritical Reynolds numbers. However, the mean drag coefficient of a sphere in VIV is about 0.8 according to Williamson et al. (1997), and suggests that the results of the experiments herein are reasonable. For $Re > 1.5 \times 10^5$, the mean drag coefficient gradually decreases as Re increases reaching 0.2 at $Re = 3 \times 10^5$. This suggests that the sudden increase in the vibration amplitude for $Re > 2.0 \times 10^5$ is closely related to the critical Reynolds number.

Figure 5 shows the dimensionless frequency f^* (defined as f/f_{nw}; where: f is the sphere's vibration frequency). The solid line in the graph shows $f^* = f_s/f_{nw}$; where: f_s is the vortex-shedding

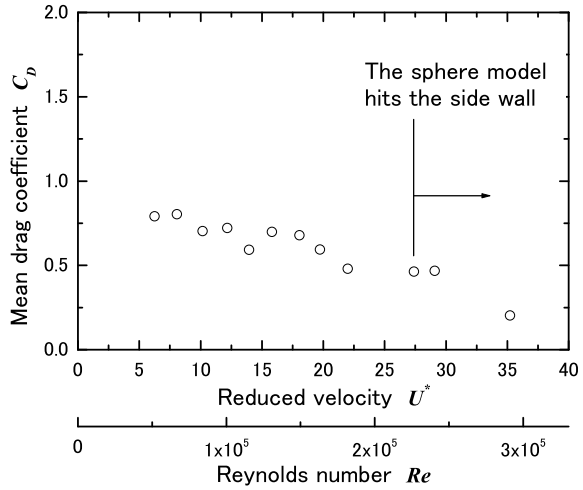

Figure 4: *Drag coefficient of sphere model A.*

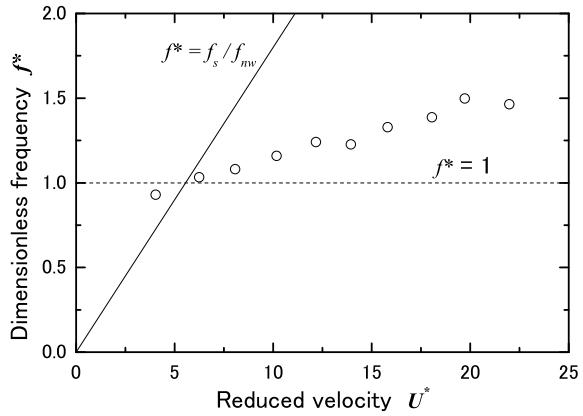

Figure 5: *Response frequency of sphere model A.*

frequency from a stationary sphere. The dimensionless frequency gradually rises with reduced velocity. This is consistent with the results of previous studies by Williamson et al. (1997) and Govardhan et al. (2005) for low mass ratio.

3.2. Results for the small sphere model B

The sphere model A contacted the side wall of the water tunnel for $U^* > 27$. Consequently, experiments for sphere model A were not conducted at higher reduced velocities to avoid damage to the test facility. In order to investigate the behavior of a tethered sphere in the higher reduced velocity range, the smaller model B was used.

Figure 6 shows the relative amplitude A_y^* versus reduced velocity and Reynolds number. Similar vibrations (performing circular or elliptical trajectories) to those for sphere model A were observed. The vibration continued in the higher reduced velocity range and, at around $U^* = 80$, the

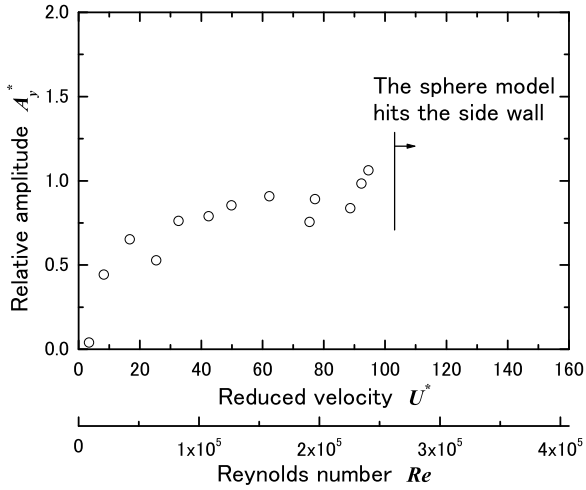

Figure 6: *Response amplitude of sphere model B.*

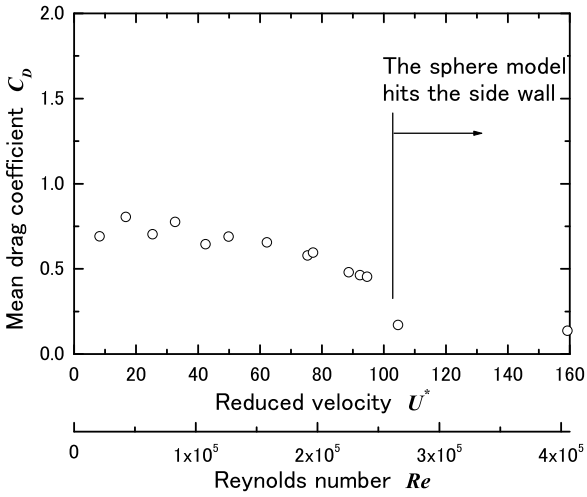

Figure 7: *Drag coefficient of sphere model B.*

relative amplitude seemed to saturate at about 1.0. However, at $U^* > 80$, the vibration became irregular. Moreover, an offset in the mean position of the sphere appeared and intermittently changed every several cycles. Finally, for $Re > 2.5 \times 10^5$, the sphere again contacted the side wall; again showing that the maximum displacement is well in excess of 4.5 times the sphere diameter.

Figure 7 shows the mean drag coefficient measured during the free vibration tests. For $4 \times 10^4 < Re < 1.5 \times 10^5$, the mean drag coefficient was about 0.7 and is reasonable for a sphere in VIV at subcritical Reynolds numbers. For $Re > 1.5 \times 10^5$, the mean drag coefficient gradually decreased as Re increased, reaching about 0.15 at $Re = 2.5 \times 10^5$. The mean drag coefficient of sphere models A and B agree well.

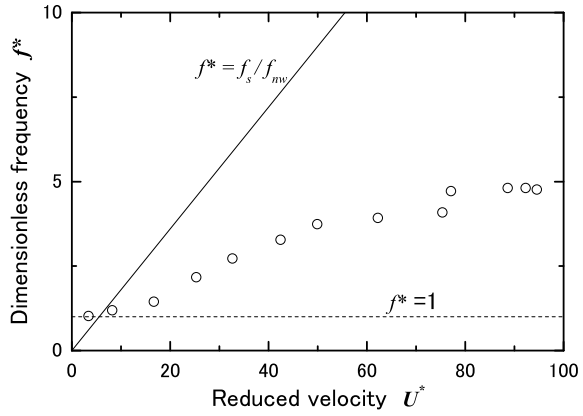

Figure 8: *Response frequency of sphere model B.*

Figure 8 shows the dimensionless frequency f^* which gradually increased with reduced velocity. Additionally, the rate of increase appears to change at around $U^* = 20$ and goes on to saturate at 5 at $U^* > 80$.

4. DISCUSSION

4.1. Vibration mechanism

According to Jauvtis et al. (2001) and Govardhan et al. (2005), FIVs of a tethered sphere can be classified into four modes. Modes I and II are vortex-induced vibrations appearing for $StU^*/f^* < 2$; where: St is the Strouhal number of a stationary sphere. A highly periodic vibration (mode III) also appears for $3 < StU^*/f^* < 8$, and is categorized in 'movement-induced vibrations' (Naudascher and Rockwell, 1994). For much higher reduced velocities, mode IV vibration can occur (Jauvtis et al., 2001). This has large amplitude and less periodicity and its mechanism is not fully understood.

In the present experiments, the periodic vibrations of sphere models A and B, as observed at $U^* < 20$, correspond to mode I and II VIV. Additionally, the vibration amplitude of sphere A was 1.5 times larger than reported in previous studies. The difference in amplitude between the present and the previous experiments is possibly caused by the difference in Reynolds number, the mass damping and the tether direction to flow. The vibration of sphere B for $20 < U^* < 100$ was presumably mode III. Though the boundary between modes II and III is not clearly distinguishable in Figures 6 - 8, the difference between the two modes does appear in the effective added mass as described in the section 4.2.

The vibration observed for $Re > 2.0 \times 10^5$ was less periodic, and may be that of mode IV as reported by Jauvtis et al. (2001). However, the vibration occurred around the critical Reynolds number for both spheres A and B, independently of the reduced velocity. The vibration amplitude was much larger than that of mode IV. Hence, the vibration is probably peculiar to the regime of critical Reynolds number, and the mechanism differs from that of mode IV. It is well known that, in the critical Reynolds number range, the flow separation point for a sphere moves aft and the wake width shrinks due to the turbulence transition of the separated shear layers. In this case, periodic vortex-shedding is not observed, and the wake tends to tilt against the flow direction, resulting in a lateral fluid force on the sphere (Taneda, 1978; Constantinescu, 2004). When a steady lateral fluid force $\bar{F}_L = \frac{1}{2}\rho_w U^2 A_\perp \bar{C}_L$ acts on a sphere, the sphere can contact with the wall for the condition:

$$\frac{\bar{F}_L}{(m_s - m_d)g + \bar{F}_D} > \frac{r - d/2}{L'} \qquad (8)$$

where r is the distance between the center of the test section and the side wall. The inequality above is obtained from the balance of steady forces on a tethered sphere. The inequality (8) is satisfied when $\bar{C}_L \geq 0.1$ and $U \geq 0.9$ m/s in case of the sphere A; and when $\bar{C}_L \geq 0.05$ and $U \geq 1.2$ m/s in case of the sphere B. In the critical Reynolds number range, 0.05∼0.1 are possible values for $\bar{C}_L$. In the experiments, the spheres do not contact the wall steadily, but vibrates against and hits the wall repeatedly. The vibration may be caused by intermittent switching of lateral force. In this case, the vibration is categorized as buffeting. The vibration may also be caused by the wake tilt synchronizing with the sphere motion. In this case, the vibration is categorized as 'movement-induced vibrations'. In either case, the vibration is probably specific to the critical Reynolds number range.

4.2. Frequency characteristics

In the same manner as Govardhan et al. (2005), the effective added mass m_{EA} is derived from the dimensionless frequency f^* as follows. Taking into account of the mean drag force $\bar{F}_D$, which increases the restoring force, the natural frequency of the present system can be expressed:

$$f = \frac{1}{2\pi}\sqrt{\frac{(m_s - m_d)g + \bar{F}_D}{(m_s + m_{EA})L'}} \qquad (9)$$

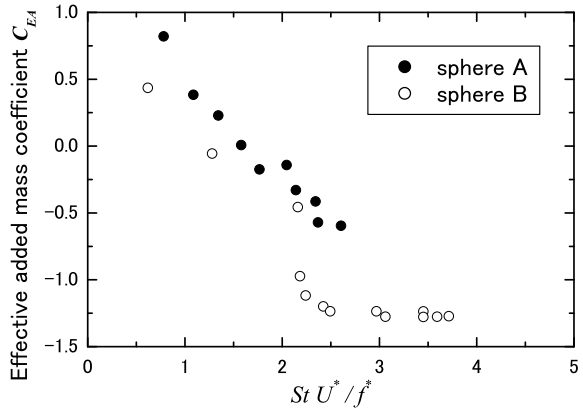

Figure 9: *Effective added mass coefficient.*

Equation (9) can be written:

$$f = \frac{1}{2\pi}\sqrt{\frac{g}{L'}\frac{m^* - 1}{m^* + C_{EA}}\left(1 + \frac{3}{4}\bar{C}_D F_r^2\right)} \qquad (10)$$

where: C_{EA} is the effective added mass coefficient, expressed: m_{EA}/m_d; and F_r is the Froude number, defined:

$$F_r^2 = \frac{U^2}{(m^* - 1)gd} \qquad (11)$$

By using eqs. (6) and (10), the effective added mass coefficient can be derived:

$$C_{EA} = \frac{m^* + C_A}{f^{*2}}\left(1 + \frac{3}{4}\bar{C}_D F_r^2\right) - m^* \qquad (12)$$

Figure 9 shows the estimated values of the effective added mass coefficients versus StU^*/f^*; where: St is 0.18 at subcritical Reynolds numbers (Achenbach, 1974). For sphere A, C_{EA} reduces with increasing StU^*/f^*, reaching about -0.6 at $StU^*/f^* = 2 \sim 2.5$. This agrees well with the results of Govardhan et al. (2005). However, for sphere B, a sudden drop in C_{EA} to about -1.2 appears at $StU^*/f^* = 2.2$ and suggests that the frequency characteristics of mode III differ from those of mode II.

5. CONCLUSIONS

Free vibration tests of a sphere tethered in a vertical water tunnel were conducted up to the critical Reynolds number. As a result, violent vibrations with unexpectedly large amplitude were observed at the critical Reynolds number. This is probably peculiar to flows in the critical Reynolds number range. At subcritical Reynolds numbers, similar sphere vibration behavior to that reported in several previous studies was observed. The results also suggest that the frequency characteristics of the vibration in the higher reduced velocity range (mode III) differ from the vortex-induced mode II vibration.

6. REFERENCES

Achenbach, E., 1972, *J. Fluid Mech.* **54**: 565-575.

Achenbach, E., 1974, *J. Fluid Mech.* **62**: 209-221.

Bearman, P.W., 1984, *Ann. Rev. Fluid Mech.* **16**: 195-222.

Blevins, R.D., 1990, *Flow-Induced Vibrations, 2nd ed.*, New York: Van Nostrand Reinhold.

Chen, S.S., 1987, *Flow-Induced Vibration of Circular Cylindrical Structures*, Washington, D.C.: Hemisphere Publishing.

Constantinescu, G. and Squires, K., 2004, *Phys. Fluids* **16**: 1449-1466.

Govardhan, R. and Williamson, C.H.K., 2005, *J. Fluid Mech.* **531**: 11-47.

King, R., 1977, *Ocean Eng.* **4**: 141-172.

Jauvtis, N. et al. 2001, *J. Fluids Struct.* **15**: 555-563.

Matsumoto, M., 1999, *J. Fluids Struct.* **13**: 791-811.

Naudascher, E., 1987, *J. Fluids Struct.* **1**: 265-298.

Naudascher, E. and Rockwell, D., 1994, *Flow-Induced Vibrations - An Engineering Guide*, Rotterdam: Balkema.

Nishihara, T. et al., 1998, *J. Wind Eng.* **77**: 23-28. (*in Japanese*)

Provansal, M. et al., 2005, *J. Flow Vis. Image Process.* **12**: 29-44.

Sarpkaya, T., 1979, *ASME J. Applied Mech.* **46**: 241-258.

Sarpkaya, T., 2004, *J. Fluids Struct.* **19**: 389-447.

Taneda, S., 1978, *J. Fluid Mech.* **85**: 187-192.

Williamson, C.H.K. and Govardhan, R.N., 1997, *J. Fluids Struct.* **11**: 293-305.

Williamson, C.H.K. and Govardhan, R.N., 2004, *Ann. Rev. Fluid Mech.* **36**: 413-455.